Quantum oscillations of the $j = 3/2$ Fermi surface in the topological semimetal YPtBi

Hyunsoo Kim [1,2,*] Junhyun Lee,[3,4,*] Halyna Hodovanets,[1,2] Kefeng Wang,[1] Jay D. Sau,[3] and Johnpierre Paglione [1,5,†]

[1]*Maryland Quantum Materials Center, Department of Physics, University of Maryland, College Park, Maryland 20742, USA*
[2]*Department of Physics, Missouri University of Science and Technology, Rolla, Missouri 65409, USA*
[3]*Department of Physics, Condensed Matter Theory Center and the Joint Quantum Institute,*
University of Maryland, College Park, Maryland 20742, USA
[4]*Department of Physics and Astronomy, Center for Materials Theory,*
Rutgers University, Piscataway, New Jersey 08854, USA
[5]*Canadian Institute for Advanced Research, Toronto, Ontario, Canada M5G 1Z8*

The bismuth-based half-Heusler materials host a nontrivial topological band structure, unconventional superconductivity, and large spin-orbit coupling in a system with very low electron density. In particular, the inversion of *p*-orbital-derived bands with an effective angular momentum j of up to 3/2 is thought to play a central role in anomalous Cooper pairing in the cubic half-Heusler semimetal YPtBi, which is thought to be the first "high-spin" superconductor. Here, we report an extensive study of the angular dependence of quantum oscillations (QOs) in the electrical conductivity of YPtBi, revealing an anomalous Shubnikov–de Haas effect consistent with the presence of a coherent $j = 3/2$ Fermi surface. The QO signal in YPtBi manifests an extreme anisotropy upon rotation of the magnetic field from the [100] to [110] crystallographic direction, where the QO amplitude vanishes. This radical anisotropy for such a highly isotropic system cannot be explained by trivial scenarios involving changes in effective mass or impurity scattering, but rather is naturally explained by the warping feature of the $j = 3/2$ Fermi surface of YPtBi, providing direct proof of active high angular momentum quasiparticles in the half-Heusler compounds.

I. INTRODUCTION

The intrinsic electron spin $s = 1/2$ and its orbital angular momentum l are often blended due to relativistic orbital motion. This spin-orbit coupling (SOC) is very strong in compounds containing heavy elements, and therefore the total angular momentum, or effective spin, j, becomes the most relevant quantum number [1–5]. Changes in the electronic band structure driven by SOC are fundamental to understanding nontrivial topology in the quantum spin Hall effect [6,7] and Weyl physics [8,9]. More recently, solid state fermionic systems with high-spin quasiparticles (i.e., j greater than 1/2) stabilized by strong SOC are gaining much attention because of this possibility of quite novel physics of interactions and their resultant exotic phases of matter [3,5]. In addition to cold-atom systems [10,11], high-spin $j = 3/2$ quasiparticles are thought to be present in the vicinity of quadratically touching bands in topological cubic materials such as the pyrochlore iridates [12], HgTe [6,7], and *R*PtBi half-Heuslers (R = rare earth) [8,9,13], antiperovskites [14,15], lacunar spinels [16,17], and Rarita-Schwinger-Weyl semimetals [18].

*H.K. and J.L. contributed equally to this work.
†paglione@umd.edu

Emergent phenomena stemming from the large j are particularly interesting in the formation of Cooper pairs and superconducting states, as the pairing of high-spin fermions challenges the conventional spin-1/2 picture of Cooper pairs by allowing pairing with arbitrary spin [1], such as $J = 2$ (quintet) and $J = 3$ (septet) pairing states recently proposed to occur in YPtBi [3,5]. Depending on their symmetry, high-spin fermionic systems are predicted to host a number of distinct superconducting phases with unique properties [19]. In systems preserving both time reversal and inversion symmetries, a nematic d wave can be imposed in the s-wave pairing channel in *cubic* compounds as the d-wave pairing causes spontaneous structural distortion [20,21]. When time reversal symmetry is broken, the system favors a quintet Weyl superconductor with a charge-neutral Bogoliubov Fermi surface as a pseudomagnetic field arises from the interband Cooper pairing [22,23]. Unorthodox mixing between quintet d wave and singlet s wave states is also expected even in a *centrosymmetric* superconductor [24,25]. When inversion symmetry is broken, a singlet-septet pairing state with topological ring-shape line nodes can be realized, which manifests a two-dimensional (2D) Majorana fluid enclosed by the surface projection of the nodal rings [4,23]. Hence high-spin superconductors serve as a potential shortcut to realizing a platform for fault-tolerant topological quantum computation.

The topological half-Heusler family *R*PtBi provides a unique platform for hosting high-spin superconductivity. Whereas the conduction and valence bands of a trivial fcc

compound are derived from the atomic *s* and *p* orbitals, respectively, strong SOC inverts these two bands producing a topologically nontrivial band structure [26–28] similar to that of HgTe [6,7]. However, knowledge of the experimental band structure has been elusive as the bulk chemical potential is inconsistent between results from angle-resolved photoemission spectroscopy (ARPES) [5,29,30] and quantum oscillation (QO) experiments [5,31]. Furthermore, different interpretations of the observed surface states from different ARPES measurements make this issue more obscure [5,29,30], and to date the proof of $j = 3/2$ quasiparticles is limited to the deduction of allowed pairing symmetries following observations of nodal quasiparticles in the superconducting state of YPtBi [5]. Together with the surprising general lack of direct experimental evidence for high-spin quasiparticles in the solid state, the need to conclusively verify the band structure and quasiparticle nature in YPtBi is of utmost importance.

In this paper, we report compelling evidence for a coherent $j = 3/2$ Fermi surface in YPtBi via studies of the angle-dependent Shubnikov–de Haas (SdH) effect. Our observation of a strikingly anisotropic variation of the amplitude of quantum oscillations in this high-symmetry compound is only compatible with a Fermi surface composed of coherent $j = 3/2$ quasiparticles, demonstrating a phenomenon that has remained elusive in other high-spin systems [12,17,18,32], including the hole-doped silicon and germanium semiconductors which have been studied thoroughly for decades. Our study offers a thorough understanding of the $j = 3/2$ fermiology in the family of RPtBi compounds, confirming their topological nature of the band structure [5] and providing a cornerstone for the realization of high-spin superconductivity and consequent quantum device applications [33,34].

II. RESULTS AND DISCUSSION

To probe the $j = 3/2$ Fermi surface, we performed a comprehensive study of SdH quantum oscillations in YPtBi single crystals grown out of molten Bi via the high-temperature flux method [5,31,35]. Electrical resistance was measured by using a standard four-probe technique in a commercial cryostat equipped with a 14-T magnet. The electrical contacts on the samples were attached by silver epoxy. A single-axis rotator was used to change the orientation of samples with respect to the direction of applied magnetic field. The orientations of the crystallographic direction were determined by using single-crystal x-ray diffraction patterns [36]. Because the transport properties of a semimetal depend sensitively on the charge carrier density n, we were careful to use only samples with a similar low-temperature value of $n \approx 2 \times 10^{18}$ cm^{-3} in this work.

Figure 1 presents the SdH effect in YPtBi with various configurations at 2 K. Figure 1(a) shows the oscillatory part of magnetoresistance ΔR which was obtained by subtracting a smoothly varying background magnetoresistance in a sample prepared out of the (001) plane (raw data are presented in the Supplemental Material [36]). In this experiment, the magnetic field was rotated from the [001] ($\theta = 0°$) to [100] direction ($\theta = 90°$) to reveal a remarkable angle-dependent
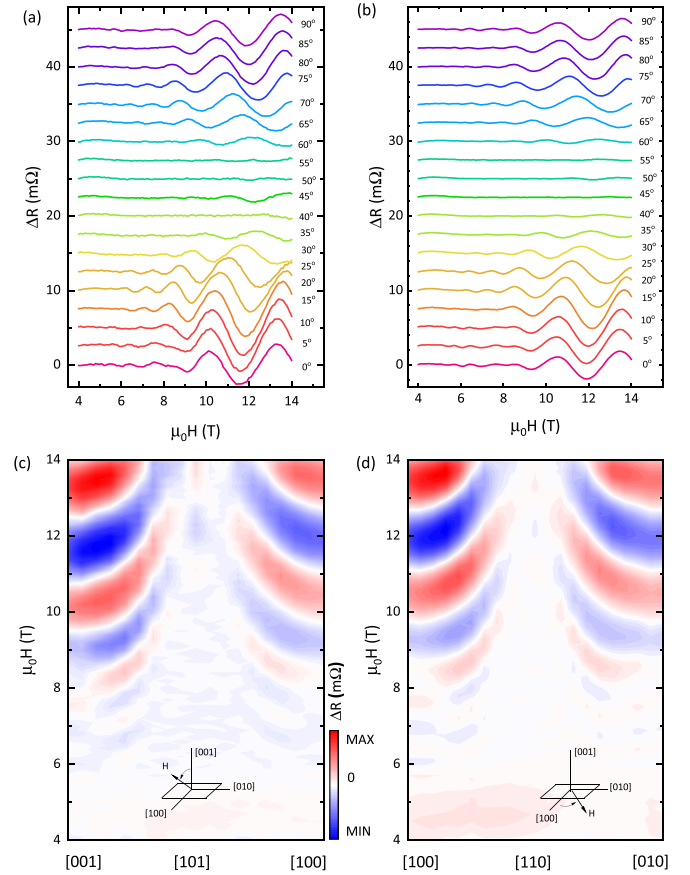

FIG. 1. Angle-dependent Shubnikov–de Haas quantum oscillations at $T = 2$ K in YPtBi. The oscillatory components $\Delta R(T)$ are presented with various field orientations (a) from [001] to [100] and (b) from [100] to [010]. Corresponding contour plots of ΔR are shown in (c) and (d), respectively, where the schematic of field rotation is shown.

amplitude with an oscillation pattern evidently symmetric about $\theta = 45°$. The QO frequency ($F \approx 45$ T) does not seem to significantly depend on the angle, which is consistent with a nearly spherical Fermi surface [5]. Figure 1(b) shows similar results from in-plane rotation experiments with the field direction from [100] to [010], consistent with the cubic symmetry.

Figures 1(c) and 1(d) display contour plots of $\Delta R(H, \theta)$ from these two rotation experiments. We assigned the crystallographic orientations on the horizontal axis, according to the fourfold crystal symmetry of YPtBi. The contour plots reveal a few key characteristics of the angle-dependent QO. Most notably, the amplitude of oscillations dramatically vanishes near the [110]-equivalent directions. Also, the oscillations move toward higher fields as approaching [110], and beating nodes were observed between $\theta = 0°$ and $\theta = 20°$ in the field range around 7 T, indicating multiple oscillatory components.

To confirm the vanishing QO amplitude along the [110] symmetry direction, a full-rotation experiment was performed on a sample cut out of the (111) plane, with a magnetic field rotated in the sample plane. In this configuration, the field direction will rotate through six [110]-equivalent
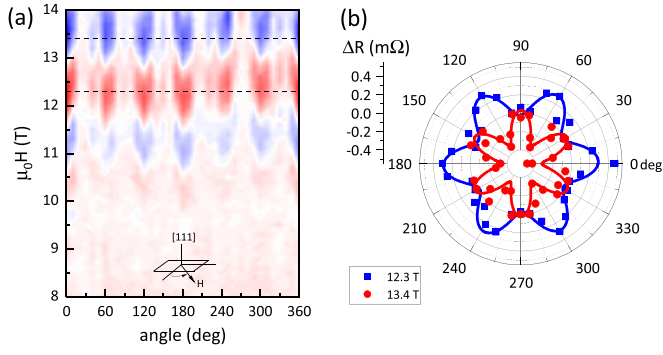
FIG. 2. Angle-dependent Shubnikov–de Haas quantum oscillations at $T = 2$ K in YPtBi with magnetic fields rotating around [111]. (a) A contour plot of ΔR with the schematic of field configuration. (b) A polar plot of ΔR for magnetic fields of 12.3 and 13.4 T [depicted in (a) with dashed lines]. Both plots clearly show a sixfold symmetry confirming the vanishing quantum oscillation amplitude in the crystallographic [110] direction of YPtBi.

directions, yielding a sixfold symmetry of $\Delta R(\theta)$ which is clearly observed as shown in Fig. 2. While the sixfold symmetry naturally follows from the cubic crystal, this result clearly confirms the vanishing QO in the [110] symmetry directions. Below we investigate the possible mechanisms behind this dramatic anisotropy.

We first address the possibility of angular variations in conventional quantities. The QO amplitude is strongly determined by the cyclotron mass m^* and impurity scattering time τ. In the semiclassical picture, QOs are observable only when the cyclotron orbit can be completed, i.e., $\omega_c \tau < 1$ where $\omega_c = e\mu_0 H/m^*$ is the cyclotron frequency. Therefore, a strong angle dependence of m^* and τ can in principle be responsible for the strong anisotropy in the observed QO amplitude. Within the standard Lifshitz-Kosevich (LK) theory [37], the oscillatory part of the longitudinal magnetoresistance $\Delta R(T, H)$ is proportional to $A_T(T, H)A_D(H)$ where

$$A_T(T, H) = \frac{\alpha T/\mu_0 H}{\sinh(\alpha T/\mu_0 H)}, \qquad (1)$$

$$A_D(H) = \exp\left(-\frac{\alpha T_D}{\mu_0 H}\right), \qquad (2)$$

with $\alpha = 2\pi^2 k_B m^*/e\hbar$ and the Dingle temperature $T_D = \hbar/2\pi k_B \tau$. Evidently, m^* and τ can be obtained from the T and H dependence of the QO amplitude. However, m^* and τ in the vicinity of the [110] direction have to be asymptotically deduced from the angular variation since there is no QO observable in that orientation.

As presented in Fig. 3(a), the temperature evolution of the QO amplitudes for various angles extracted from the fast Fourier transform spectra [36] show little variation, as reflected in the lack of angular dependence of the extracted values of m^* shown in Fig. 3(b). Likewise, the scattering time τ determined from the field variation of the QO amplitudes only moderately depends on the angle as shown in Fig. 3(d), pointing to only marginal effects on the QO amplitude between [100] and [110] and allowing us to rule
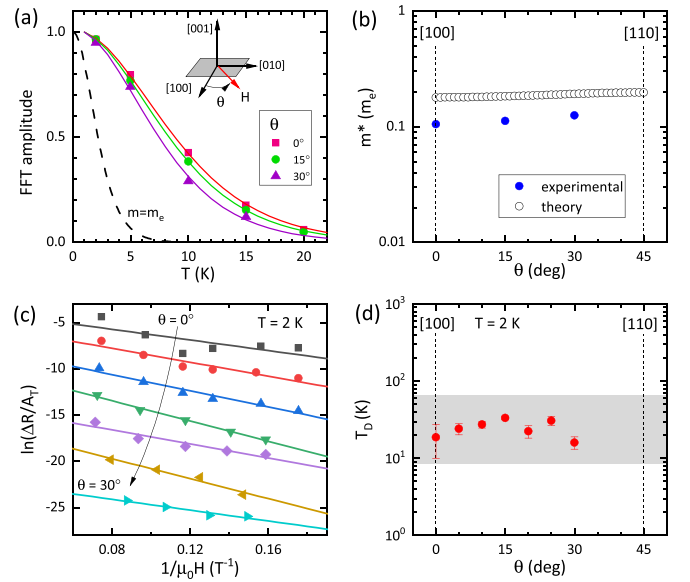

FIG. 3. Angle-dependent cyclotron mass m^* and impurity scattering time τ in YPtBi. (a) Temperature dependence of the normalized QO amplitude. Symbols represent experimental values, and the solid lines represent the best theoretical fit with the LK formula $A_T(T, H)$ [Eq. (1)]. (b) Angle-dependent m^* obtained from the experimental results (solid symbols) by using Eq. (1) and the theoretical investigation (open symbols) within the the $\mathbf{k} \cdot \mathbf{p}$ Hamiltonian model. (c) Field-dependent QO amplitude at $T = 2$ K. The symbols represent experimental values between $\theta = 0°$ and $30°$ and the solid straight lines represent a linear fit $(-a/\mu_0 H + b)$ to the LK formula $A_D(H)$ [Eq. (2)]. (d) Angle-dependent T_D determined from the linear fit in (c).

out their accounting for the abrupt vanishing of QO unless a nearly discontinuous change occurs between $30°$ and $45°$. Although the diverging effective mass was observed in some unconventional superconductors in the vicinity of a quantum critical point [38,39], this scenario is not plausible for YPtBi which is a low-carrier semimetal [31,35].

Apart from the $A_T(T, H)A_D(H)$ factor, the QO amplitude fundamentally depends on the density of states contributing to the extremal QO orbits. In the LK formula [37], this effect is included as a prefactor $[\partial^2_{\tilde{k}_\parallel} S(\tilde{k}_\parallel)]^{-1/2}$ of the amplitude of QO. Here, S is the cross-section area of the Fermi surface perpendicular to $k_\parallel$, the momentum parallel to the external field, and $\tilde{k}_\parallel$ indicates the value of $k_\parallel$ where the Fermi-surface area is an extrema [40]. The strong angle dependence of $[\partial^2_{\tilde{k}_\parallel} S(\tilde{k}_\parallel)]^{-1/2}$ could result in a drastic change in the QO amplitude upon rotation. This effect has been well demonstrated in systems with a corrugated 2D Fermi surface [38,41,42], but has been overlooked in 3D systems.

To determine the angular variation of $[\partial^2_{\tilde{k}_\parallel} S(\tilde{k}_\parallel)]^{-1/2}$, we construct the Fermi surface within the four-band $\mathbf{k} \cdot \mathbf{p}$ model for spin $j = 3/2$ electrons that is written as [3,12,43–45]

$$\mathcal{H}_0 = Ak^2 + B\sum_i k_i^2 J_i^2 + C\sum_{i \neq j} k_i k_j J_i J_j$$
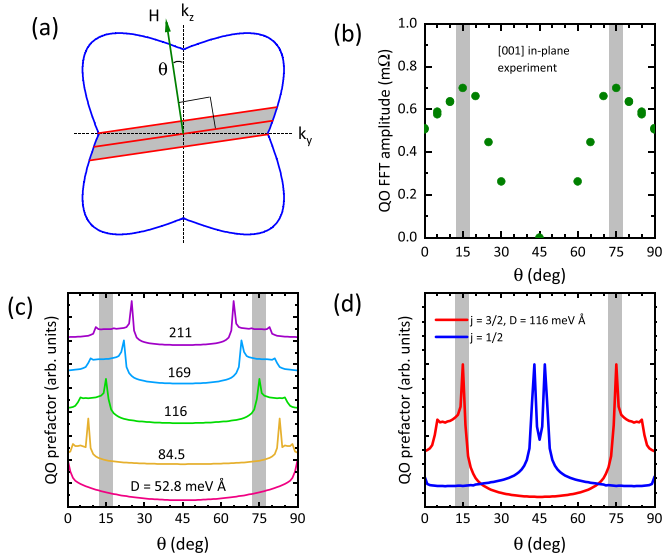$$+ D\sum_i k_i(J_{i+1}J_i J_{i+1} + J_{i+2}J_i J_{i+2}). \qquad (3)$$

FIG. 4. Angular variation of the prefactor $[\partial_{\tilde{k}_\parallel}^2 S(\tilde{k}_\parallel)]^{-1/2}$ of the QO amplitude. (a) A schematic cross section of the $j = 3/2$ Fermi surface, where the warping sensitively depends on D [see Eq. (3)]. The red lines and gray band represent the cyclotron orbits and the enhanced density of states on the Fermi surface perpendicular to the applied field H, when the quantum oscillation amplitude is maximum. (b) The angle-dependent QO amplitude calculated from fast Fourier transform. Note the maximum amplitude around 15°. (c) The angular variation of the outer Fermi surface's $[\partial_{\tilde{k}_\parallel}^2 S(\tilde{k}_\parallel)]^{-1/2}$ with different choices of D. The gray vertical bars represent the maximum amplitude of experimental QO shown in (b). (d) Angular variation of $[\partial_{\tilde{k}_\parallel}^2 S(\tilde{k}_\parallel)]^{-1/2}$ of $j = 1/2$ and $j = 3/2$ outer Fermi surfaces. The position of the maximum and overall tendency of $j = 3/2$ theory show reasonable agreement with the experimental QO amplitude results.

Here, J_i's are the ith directional $j = 3/2$ angular momentum operator, and we used $A = 22.9$ eV Å^2, $B = -20.7$ eV Å^2, $C = -14.2$ eV Å^2, and $D = 0.116$ eV Å, which are previously determined in YPtBi [46]. The chemical potential of $\mu = -35$ meV, corresponding to the observed QO frequency $F = 45$ T [5,31], is used in the following calculations. Equation (3) gives a spin-split band structure, with only the principal axes being degenerate due to the C_2 rotational symmetries around the principal axes. The spin-split band structure with degenerate principal axes results in the bulging of the Fermi surface in the [111] direction. A schematic 2D projection of the warped Fermi surface of YPtBi with $k_z = 0$ is depicted in Fig. 4(a). One can find that D in Eq. (3) is the dominant factor for the warping and therefore significantly affects the angular variation of $[\partial_{\tilde{k}_\parallel}^2 S(\tilde{k}_\parallel)]^{-1/2}$.

In Fig. 4(c), we calculate the QO prefactor $[\partial_{\tilde{k}_\parallel}^2 S(\tilde{k}_\parallel)]^{-1/2}$ of the outer Fermi surface as a function of θ for different values of D. For $D \geqslant 84.5$ meV Å, the prefactor clearly exhibits sharp peaks whose angular position depends on the choice of D. We note that the prefactor contribution from the inner Fermi surface does not exhibit strong angular modulation [36], and therefore the outer Fermi surface is likely responsible for the observed anisotropy in the QO ampli-

tude. We found that $[\partial_{\tilde{k}_\parallel}^2 S(\tilde{k}_\parallel)]^{-1/2}$ exhibits the minimum value at $\theta = 45°$ with all tested D values, which suggests that the absence of QOs around the [110]-equivalent directions stems from the intrinsic properties of the Fermi surface in YPtBi.

It is noteworthy that in YPtBi, apart from the vanishing amplitude in the [110]-equivalent directions, the QO signal is strongest around $\theta = 15°$. We fine-tuned D to match the experimental enhancement of QO [Fig. 4(b)] and found that $D = 116$ meV Å best agrees with the experiment. We plot the QO prefactor with $D = 116$ meV Å together with that of the hypothetical Fermi surface with $j = 1/2$ in Fig. 4(d). Whereas the $j = 3/2$ Fermi surface exhibits a minimum near 45°, the $j = 1/2$ Fermi surface produces *peaks* near the [110] direction, which is a result of the $j = 1/2$ band structure having additional degenerate lines along the [111] direction [36]. Moreover, the angle-dependent Zeeman energy leads to a selective interorbit hopping during cyclotron motion, which additionally weakens the QO amplitude with a magnetic field near the [110] direction. This effect is discussed in the Supplemental Material [36] in detail. Combining both effects, the angle dependence of QO reasonably captures the $j = 3/2$ nature of the Fermi surface in YPtBi. While the theoretical QO prefactor grossly follows the angular variation of the experimental QO amplitude, we do not expect quantitative agreement between the two because of the other factors contributing to QO, which include the effective mass and scattering rate. Theoretical calculation of the QO amplitude would require additional artificial assumptions and it is beyond the scope of the current work. However, we emphasize that we successfully single out the factor resulting in the key features of the QO experiment without calculating the full QO amplitude.

III. SUMMARY

In summary, we report an unexpected extreme amplitude variation of the quantum oscillations upon rotation of a magnetic field in YPtBi, a novel low-carrier density topological semimetal that has been identified as a potential high-spin "septet" superconductor [5]. Upon rotating a magnetic field, the observed quantum oscillations of this nearly spherical Fermi-surface system vanish when the field is directed along the [110]-equivalent crystallographic directions and reach a maximum at $\theta \approx 15°$ from the [100] direction on the (001) plane. As discussed, these observations cannot be explained by angular variations of effective mass or impurity scattering, but rather are naturally explained by properly understanding the effect of $j = 3/2$ quasiparticles forming a coherent Fermi surface in YPtBi. Our work therefore confirms the high-spin nature of the topological band structure in this material, and most likely all of the closely related half-Heusler RPtBi and RPdBi [47] compounds, and provides an advance in understanding novel spin-3/2 systems in the solid state.

ACKNOWLEDGMENTS

[1] T.-L. Ho and S. Yip, Pairing of Fermions with Arbitrary Spin, Phys. Rev. Lett. **82**, 247 (1999).

[2] C. Wu, J.-P. Hu, and S.-C. Zhang, Exact SO(5) Symmetry in the Spin-3/2 Fermionic System, Phys. Rev. Lett. **91**, 186402 (2003).

[3] P. M. R. Brydon, L. Wang, M. Weinert, and D. F. Agterberg, Pairing of $j = 3/2$ Fermions in Half-Heusler Superconductors, Phys. Rev. Lett. **116**, 177001 (2016).

[4] W. Yang, T. Xiang, and C. Wu, Majorana surface modes of nodal topological pairings in spin-$\frac{3}{2}$ semimetals, Phys. Rev. B **96**, 144514 (2017).

[5] H. Kim, K. Wang, Y. Nakajima, R. Hu, S. Ziemak, P. Syers, L. Wang, H. Hodovanets, J. D. Denlinger, P. M. R. Brydon, D. F. Agterberg, M. A. Tanatar, R. Prozorov, and J. Paglione, Beyond triplet: Unconventional superconductivity in a spin-3/2 topological semimetal, Sci. Adv. **4**, eaao4513 (2018).

[6] B. A. Bernevig, T. L. Hughes, and S.-C. Zhang, Quantum spin Hall effect and topological phase transition in HgTe quantum wells, Science **314**, 1757 (2006).

[7] M. König, S. Wiedmann, C. Brüne, A. Roth, H. Buhmann, L. W. Molenkamp, X.-L. Qi, and S.-C. Zhang, Quantum spin Hall insulator state in HgTe quantum wells, Science **318**, 766 (2007).

[8] M. Hirschberger, S. Kushwaha, Z. Wang, Q. Gibson, S. Liang, C. A. Belvin, B. A. Bernevig, R. J. Cava, and N. P. Ong, The chiral anomaly and thermopower of Weyl fermions in the half-Heusler GdPtBi, Nat. Mater. **15**, 1161 (2016).

[9] T. Suzuki, R. Chisnell, A. Devarakonda, Y. T. Liu, W. Feng, D. Xiao, J. W. Lynn, and J. G. Checkelsky, Large anomalous Hall effect in a half-Heusler antiferromagnet, Nat. Phys. **12**, 1119 (2016).

[10] C. Wu, Hidden symmetry and quantum phases in spin-3/2 cold atomic systems, Mod. Phys. Lett. B **20**, 1707 (2006).

[11] I. Kuzmenko, T. Kuzmenko, Y. Avishai, and M. Sato, Spin-orbit coupling and topological states in an $F = \frac{3}{2}$ cold Fermi gas, Phys. Rev. B **98**, 165139 (2018).

[12] E.-G. Moon, C. Xu, Y. B. Kim, and L. Balents, Non-Fermi-Liquid and Topological States with Strong Spin-Orbit Coupling, Phys. Rev. Lett. **111**, 206401 (2013).

[13] K. Manna, Y. Sun, L. Muechler, J. Kübler, and C. Felser, Heusler, Weyl and Berry, Nat. Rev. Mater. **3**, 244 (2018).

[14] T. Kawakami, T. Okamura, S. Kobayashi, and M. Sato, Topological crystalline materials of $J = 3/2$ electrons: Antiperovskites, Dirac Points, And High Winding Topological Superconductivity, Phys. Rev. X **8**, 041026 (2018).

[15] Y. Fang and J. Cano, Higher-order topological insulators in antiperovskites, Phys. Rev. B **101**, 245110 (2020).

[16] M. Y. Jeong, S. H. Chang, B. H. Kim, J.-H. Sim, A. Said, D. Casa, T. Gog, E. Janod, L. Cario, S. Yunoki, M. J. Han, and J. Kim, Direct experimental observation of the molecular $J_{\text{eff}} = 3/2$ ground state in the lacunar spinel $GaTa_4Se_8$, Nat. Commun. **8**, 782 (2017).

[17] M. J. Park, G. Sim, M. Y. Jeong, A. Mishra, M. J. Han, and S. Lee, Pressure-induced topological superconductivity in the spin–orbit Mott insulator $GaTa_4Se_8$, npj Quantum Mater. **5**, 41 (2020).

[18] I. Boettcher, Interplay of Topology and Electron-Electron Interactions in Rarita-Schwinger-Weyl Semimetals, Phys. Rev. Lett. **124**, 127602 (2020).

[19] J. W. F. Venderbos, L. Savary, J. Ruhman, P. A. Lee, and L. Fu, Pairing States of Spin-$\frac{3}{2}$ Fermions: Symmetry-Enforced Topological Gap Functions, Phys. Rev. X **8**, 011029 (2018).

[20] I. Boettcher and I. F. Herbut, Unconventional Superconductivity in Luttinger Semimetals: Theory of Complex Tensor Order and the Emergence of the Uniaxial Nematic State, Phys. Rev. Lett. **120**, 057002 (2018).

[21] G. B. Sim, A. Mishra, M. J. Park, Y. B. Kim, G. Y. Cho, and S. Lee, Topological $d + s$ wave superconductors in a multiorbital quadratic band touching system, Phys. Rev. B **100**, 064509 (2019).

[22] D. F. Agterberg, P. M. R. Brydon, and C. Timm, Bogoliubov Fermi Surfaces in Superconductors with Broken Time-Reversal Symmetry, Phys. Rev. Lett. **118**, 127001 (2017).

[23] C. Timm, A. P. Schnyder, D. F. Agterberg, and P. M. R. Brydon, Inflated nodes and surface states in superconducting half-Heusler compounds, Phys. Rev. B **96**, 094526 (2017).

[24] J. Yu and C.-X. Liu, Singlet-quintet mixing in spin-orbit coupled superconductors with $j = \frac{3}{2}$ fermions, Phys. Rev. B **98**, 104514 (2018).

[25] J. Yu and C.-X. Liu, Spin susceptibility, upper critical field, and disorder effect in $j = 3/2$ superconductors with singletquintet mixing, J. Appl. Phys. **128**, 063904 (2020).

[26] S. Chadov, X. Qi, J. Kübler, G. H. Fecher, C. Felser, and S. C. Zhang, Tunable multifunctional topological insulators in ternary Heusler compounds, Nat. Mater. **9**, 541 (2010).

[27] H. Lin, L. A. Wray, Y. Xia, S. Xu, S. Jia, R. J. Cava, A. Bansil, and M. Z. Hasan, Half-Heusler ternary compounds as new multifunctional experimental platforms for topological quantum phenomena, Nat. Mater. **9**, 546 (2010).

[28] D. Xiao, Y. Yao, W. Feng, J. Wen, W. Zhu, X.-Q. Chen, G. M. Stocks, and Z. Zhang, Half-Heusler Compounds as a New Class of Three-Dimensional Topological Insulators, Phys. Rev. Lett. **105**, 096404 (2010).

[29] C. Liu, Y. Lee, T. Kondo, E. D. Mun, M. Caudle, B. N. Harmon, S. L. Bud'ko, P. C. Canfield, and A. Kaminski, Metallic surface electronic state in half-Heusler compounds RPtBi ($R = $ Lu, Dy, Gd), Phys. Rev. B **83**, 205133 (2011).

[30] Z. K. Liu, L. X. Yang, S.-C. Wu, C. Shekhar, J. Jiang, H. F. Yang, Y. Zhang, S.-K. Mo, Z. Hussain, B. Yan, C. Felser, and Y. L. Chen, Observation of unusual topological surface states in half-Heusler compounds LnPtBi (Ln = Lu, Y), Nat. Commun. **7**, 12924 (2016).

[31] N. P. Butch, P. Syers, K. Kirshenbaum, A. P. Hope, and J. Paglione, Superconductivity in the topological semimetal YPtBi, Phys. Rev. B **84**, 220504(R) (2011).

[32] H.-S. Kim, J. Im, M. J. Han, and H. Jin, Spin-orbital entangled molecular j_{eff} states in lacunar spinel compounds, Nat. Commun. **5**, 3988 (2014).

[33] A. Kitaev, Fault-tolerant quantum computation by anyons, Ann. Phys. **303**, 2 (2003).

[34] J. D. Sau, D. J. Clarke, and S. Tewari, Controlling non-Abelian statistics of Majorana fermions in semiconductor nanowires, Phys. Rev. B **84**, 094505 (2011).

[35] P. C. Canfield, J. D. Thompson, W. P. Beyermann, A. Lacerda, M. F. Hundley, E. Peterson, Z. Fisk, and H. R. Ott, Magnetism and heavy fermion-like behavior in the RBiPt series, J. Appl. Phys. **70**, 5800 (1991).

[36] See Supplemental Material at http://link.aps.org/supplemental/10.1103/PhysRevResearch.4.033169 for the angular dependence of the prefactor contribution from the inner Fermi surface.

[37] D. Shoenberg, *Magnetic Oscillations in Metals* (Cambridge University Press, London, 1984).

[38] B. J. Ramshaw, S. E. Sebastian, R. D. McDonald, J. Day, B. S. Tan, Z. Zhu, J. B. Betts, R. Liang, D. A. Bonn, W. N. Hardy, and N. Harrison, Quasiparticle mass enhancement approaching optimal doping in a high-T_c superconductor, Science **348**, 317 (2015).

[39] K. Hashimoto, K. Cho, T. Shibauchi, S. Kasahara, Y. Mizukami, R. Katsumata, Y. Tsuruhara, T. Terashima, H. Ikeda, M. A. Tanatar, H. Kitano, N. Salovich, R. W. Giannetta, P. Walmsley, A. Carrington, R. Prozorov, and Y. Matsuda, A sharp peak of the zero-temperature penetration depth at optimal composition in BaFe$_2$(As$_{1-x}$P$_x$)$_2$, Science **336**, 1554 (2012).

[40] The Lifshitz-Kosevich formula only takes into account the second-order term of the curvature and thus has a limitation in the case of YPtBi. However, the qualitative features persist and are sufficient to discuss the key features.

[41] K. Yamaji, On the angle dependence of the magnetoresistance in quasi-two-dimensional organic superconductors, J. Phys. Soc. Jpn. **58**, 1520 (1989).

[42] S. E. Sebastian, N. Harrison, F. F. Balakirev, M. M. Altarawneh, P. A. Goddard, R. Liang, D. A. Bonn, W. N. Hardy, and G. G. Lonzarich, Normal-state nodal electronic structure in underdoped high-T_c copper oxides, Nature (London) **511**, 61 (2014).

[43] G. Dresselhaus, Spin-orbit coupling effects in zinc blende structures, Phys. Rev. **100**, 580 (1955).

[44] J. M. Luttinger, Quantum theory of cyclotron resonance in semiconductors: General theory, Phys. Rev. **102**, 1030 (1956).

[45] J. Cano, B. Bradlyn, Z. Wang, M. Hirschberger, N. P. Ong, and B. A. Bernevig, Chiral anomaly factory: Creating Weyl fermions with a magnetic field, Phys. Rev. B **95**, 161306(R) (2017).

[46] The parameter values were adjusted based on the prior publications [3,5] to best describe the experimental SdH data.

[47] Y. Nakajima, R. Hu, K. Kirshenbaum, A. Hughes, P. Syers, X. Wang, K. Wang, R. Wang, S. R. Saha, D. Pratt, J. W. Lynn, and J. Paglione, Topological RPdBi half-Heusler semimetals: A new family of noncentrosymmetric magnetic superconductors, Sci. Adv. **1**, e1500242 (2015).

Supplemental Material for "Anomalous Quantum Oscillations in Spin-3/2 Topological Semimetal YPtBi"

Hyunsoo Kim,[1, 2, †] Junhyun Lee,[3, 4, †] Halyna Hodovanets,[1, 2]
Kefeng Wang,[1] Jay D. Sau,[3] and Johnpierre Paglione[1, 5, *]

[1] *Maryland Quantum Materials Center, Department of Physics,*
University of Maryland, College Park, MD 20742, USA
[2] *Department of Physics, Missouri University of Science and Technology, Rolla, MO 65409, USA*
[3] *Department of Physics, Condensed Matter Theory Center and the Joint Quantum Institute,*
University of Maryland, College Park, Maryland 20742, USA
[4] *Department of Physics and Astronomy, Center for Materials Theory,*
Rutgers University, Piscataway, NJ 08854, USA
[5] *Canadian Institute for Advanced Research, Toronto, Ontario M5G 1Z8, Canada*
(Dated: August 11, 2022)

SINGLE CRYSTAL X-RAY DIFFRACTION PATTERN

To determine the crystallographic orientations of the samples, we performed single-crystal X-ray diffraction measurements at room temperature by using a *Rigaku Miniflex* diffractometer with Cu $K\alpha$ radiation. Diffraction patterns were taken on single crystals with a typical thickness of 25 μm. Fig. S1 (a) and (b) show the diffraction patterns from the sample cut out of the crystallographic (001)- and (111)-planes, respectively. The sharp peaks in each sample indicate a well-oriented crystallographic direction.

ANGLE-DEPENDENT MAGNETORESISTANCE AND SHUBNIKOV-DE HAAS EFFECT

Fig. S2 shows angle-dependent magnetoresistance $R(H)$ and the Shubnikov-de Haas effect (SdH) in YPtBi. The sample for this experiment was cut out of the (001)-plane, which was confirmed by the single-crystal diffraction pattern (see Fig. S1). Fig. S2(a) shows the angular variation of magnetoresistance $R(H)$ at $T = 2$ K with the magnetic field rotating from [001] to [100] with the electrical current I along [010]. The SdH effect is readily visible at the high field regime at almost all angles. The first derivative $dR/d(\mu_0 H)$ is shown in Fig. S2(b). While the sample exhibits strong quantum oscillations at high magnetic fields, the oscillation dramatically vanishes near 45°, which is the crystallographic [101]-direction. A similar experiment was performed with the rotating field from [100] to [010], keeping the direction of the electric field along [010]-direction. The angle-dependent R and $dR/d(\mu_0 H)$ are displayed in panels (c) and (d), respectively. This rotation experiment shows an almost identical angular variation with an
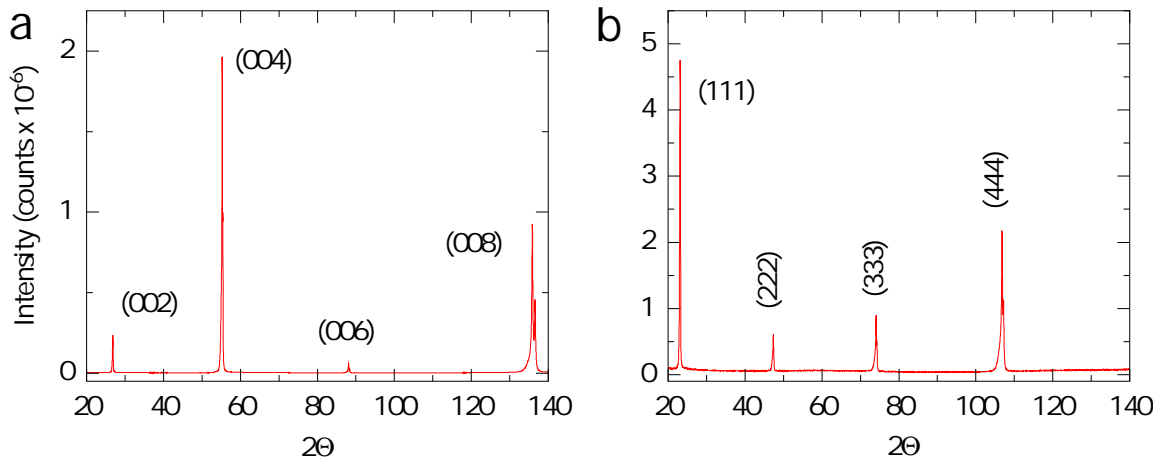

FIG. S1. Single crystal X-ray diffraction pattern in YPtBi at room temperature. (a) Sample cut out of the crystallographic (001)-plane, (b) crystallographic (111)-plane.
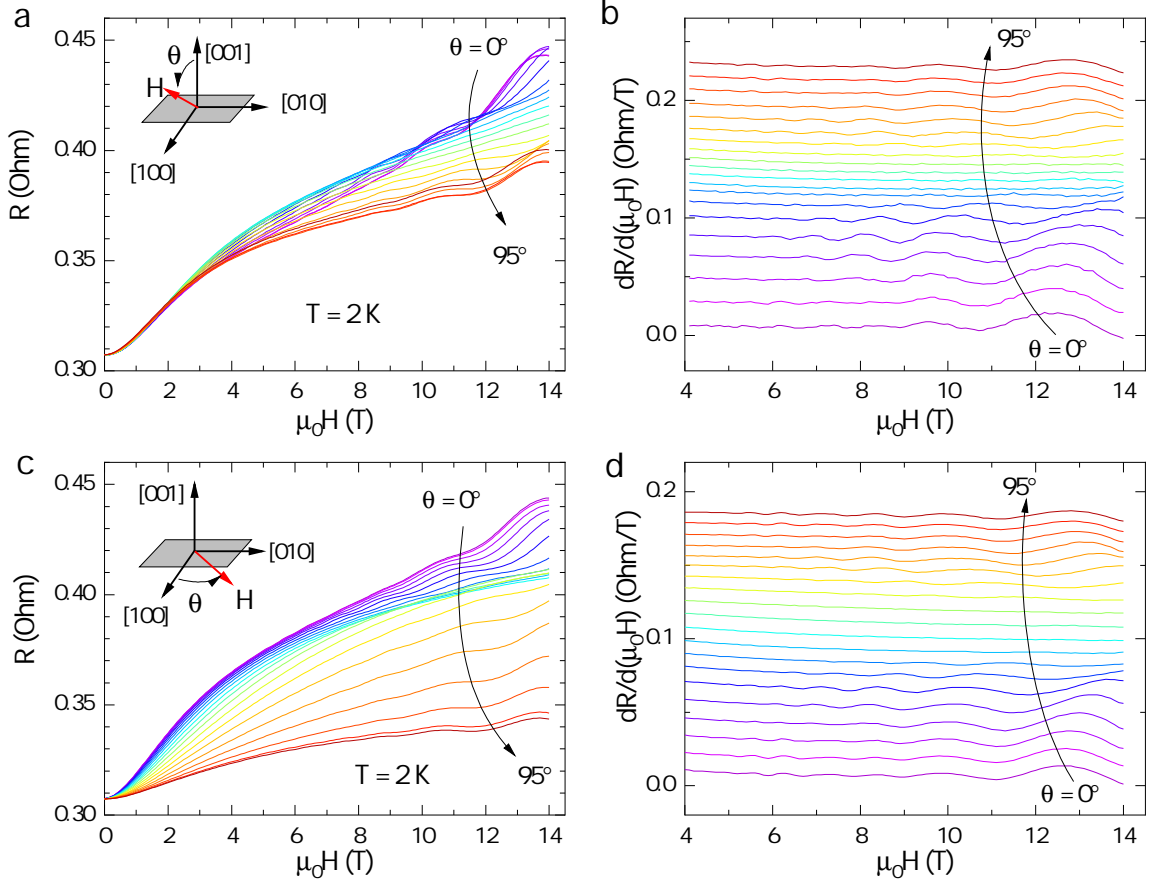
FIG. S2. Angle-dependent magnetoresistance $R(H)$ and Shubnikov-de Haas effect in the YPtBi sample with the crystallographic (001)-plane. (a) $R(H)$ with various angles θ measured from the crystallographic [001]-direction. The applied magnetic field remains transverse to the electric current direction (crystallographic [010]-direction). (b) Angle-dependent $dR/d(\mu_0 H)$ of $R(H)$ in panel (a). (c) $R(H)$ with various angles θ measured from the crystallographic [100]-direction. The applied magnetic field lies in the sample plane. (d) Angle-dependent $dR/d(\mu_0 H)$ of $R(H)$ in panel (c).

absence of the SdH effect near [110]. This suggests that the Hall contribution is negligible in the system. Therefore, while quantum oscillation in conductivity is the relevant quantity, in our case the analysis of oscillation in resistivity is sufficient.

To confirm the vanishing quantum oscillation near the crystallographic [110]-equivalent directions, another sample was prepared out of the (111)-plane. The magnetic field was rotated in the plane in which case the magnetic field will encounter six [110]-equivalent directions, i.e., the six-fold rotational symmetry with the six vanishing-angles. Fig. S3(a) shows $R(H)$ at various angles from 0° to 180° and from 180° to 360°in the left and right panel, respectively. Panel (b) shows the oscillatory component $\Delta R(H)$ after subtracting the background magnetoresistance, and $\Delta R(H)$ clearly exhibits a regular pattern upon rotation. The contour plot and $\Delta R(\theta)$ shown in Fig. 2(a) in the main text manifest the six-fold symmetry with vanishing SdH effect near the [110]-equivalent directions.

We note that the QO frequency with a magnetic field along the [111]-direction is about 56 T which is more than twofold greater than the QO frequency reported in [1]. We attribute the discrepancy to the sample dependence, and we use only the screened samples with a similar transport behavior in the main text.

FAST FOURIER TRANSFORM

The oscillatory part of the longitudinal magnetoresistance $\Delta R(H)$ is obtained by subtracting smoothly varying background $R(H)$ at various temperatures. The angle-dependent $\Delta R(H)$ at various temperatures is shown in Fig. S4(a-c). The rotation and the angle are indicated in the inset of panel (a). The quantum oscillation is strongest at 15° and
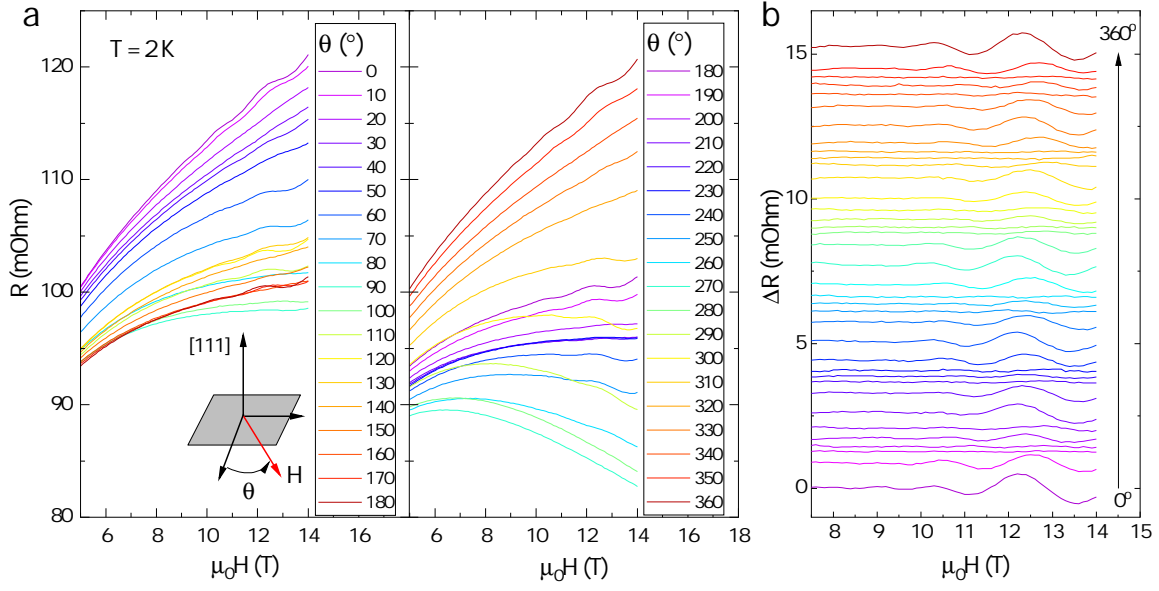
FIG. S3. Angle-dependent magnetoresistance $R(H)$ and Shubnikov-de Haas effect in the YPtBi sample with the crystallographic (111)-plane. (a) Left: $R(H)$ with various angles θ from $0°$ to $180°$, as indicated in the inset. Right: the field rotation with various angles θ from $180°$ to $360°$. The applied magnetic field lies in the sample plane, (111). (b) Angle-dependent quantum oscillation $\Delta R(H)$ from the full-rotation experiments shown in panel (a).
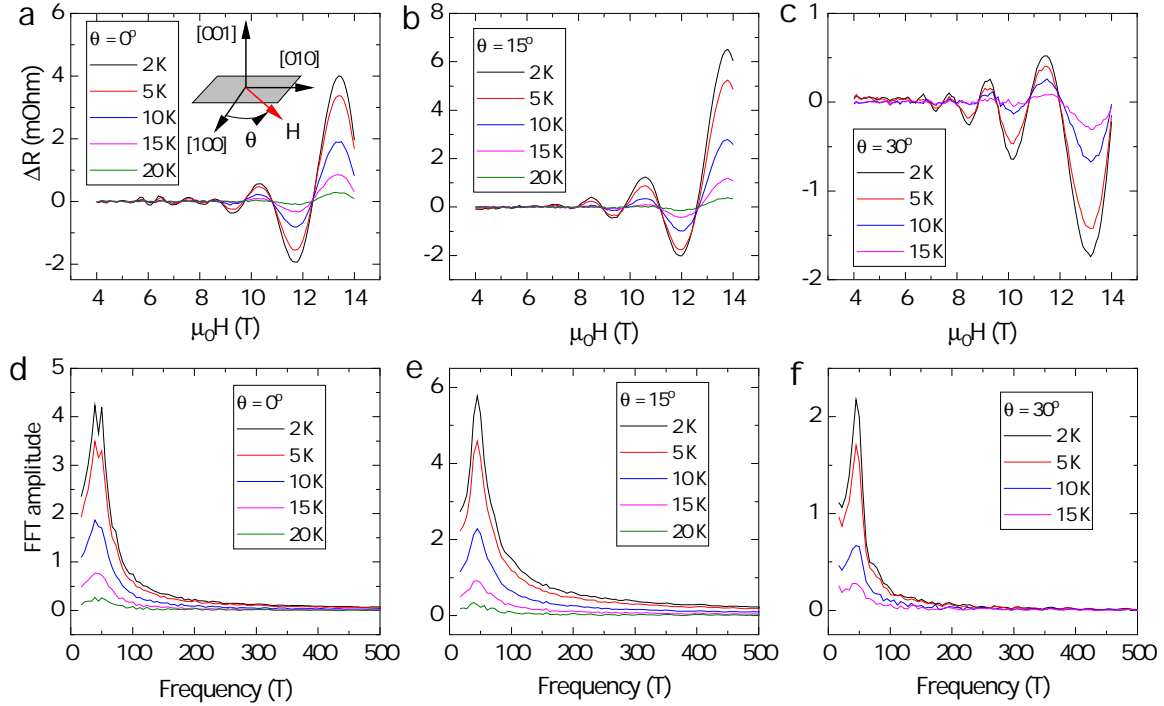

FIG. S4. Angle-dependent quantum oscillations $\Delta R(H)$ at various temperatures and its fast Fourier transform (FFT) in an YPtBi sample with the crystallographic (001)-plane. $\Delta R(H)$ with various angles θ for (a) $0°$, (b) $15°$, (c) $30°$. FFT spectra at various temperatures are shown in (d) $\theta = 0°$, (e) $15°$, (f) $30°$.
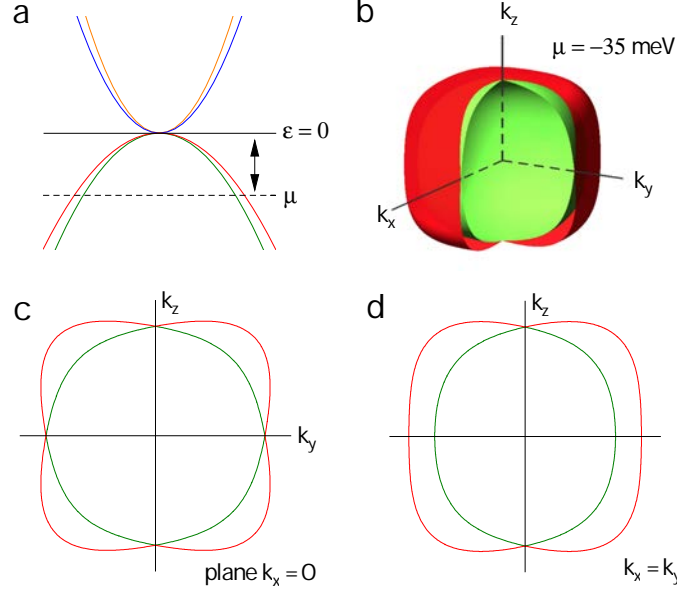
FIG. S5. Luttinger-Kohn type $j = 3/2$ band structure and Fermi surface. (a) A schematic of quadratically touching bands without inversion symmetry. The chemical potential μ is below the touching point and the red (green) band comprises the outer (inner) Fermi surface in the following figures with the same color scheme. (b) The spin-split Fermi surface from the $\mathbf{k} \cdot \mathbf{p}$ Hamiltonian [Eq. (3) in the main text] with $\mu = -35$ meV. (c) Fermi surface cross-sections for $k_x = 0$ or (100) plane, (d) for $k_x = k_y$ or (110) plane. For (c) and (d) the parameters are chosen to exaggerate the features for visibility.

much weaker at $30°$. To compare the oscillation amplitude at various angles, we employ the fast Fourier transform (FFT). The resultant FFT-spectra of the quantum oscillation at various temperatures are presented in the panels (d-f), which show the non-monotonic angular variation of the oscillation amplitude. When the angle is greater than $30°$, the oscillation drastically disappears and this FFT analysis is practically impossible.

ANISOTROPY OF THE QUANTUM OSCILLATION

The band structure and the Fermi surface of the four-band $\mathbf{k} \cdot \mathbf{p}$ model for spin $j = 3/2$ electrons [Eq. (3) of the main text] is shown in Fig. S5. The antisymmetric SOC (the term proportional to D in Eq. (3) of the main text) due to lack of inversion symmetry in the T_d point group lifts the spin-degeneracy and thus gives the spin-split Fermi surface. However, the degeneracy is preserved along the principal axes by the little group SD_{16} [2]. The degeneracy and the resulting bulges in the [111]-direction can be seen in the Fermi surface and cross sections corresponding to $k_x = 0$ and $k_x = k_y$ planes [Fig. S5(b-d)].

Our understanding of the anomalous QOs requires us to add a Zeeman interaction term to $\mathcal{H}_0$; $\mathcal{H} = \mathcal{H}_0 + \mathcal{H}_Z$ where $\mathcal{H}_Z = g\mathbf{H} \cdot \mathbf{J}$, with g being the Landé g-factor and $\mathbf{H}$ the Zeeman field. The spin-degeneracy at the principal axes are in general lifted due to this Zeeman term. We assume the field configuration as in Fig. 1(d) in the main text and calculate the minimum Zeeman gap Δ between the two bands in the vicinity of the principal axis. As shown in Fig. S6(a), Δ exhibits strong angle dependence of $\mathbf{H}$ and surprisingly vanishes when $\mathbf{H}$ is applied along [110] equivalent directions. Consequently, the degeneracy at [001] axis without the field re-appears only at the corresponding angles; this time slightly away from the [001] axis. Fig. S6(b) displays the angular evolution of the Fermi surface extrema for the plane perpendicular to $\mathbf{H}$, which shows the Fermi surface crossing (and thus the degeneracy at the crossing point) when $\theta = 45°$. The vanishing of Zeeman gap is independent of the choice of g between 2 and 40, implying a robust feature of our system.

Two representative cyclotron orbits are shown in Fig. S6(c) for $\theta = 0°$ and $45°$ following the previous observation. For $\theta = 0°$, there are two well separated cyclotron orbits with nearly zero hopping probability between inner and outer orbits in the typical laboratory field range. However, the inter-orbit transition probability increases with $\mathbf{H}$ tilting away from $0°$ as two orbits approaches closer, and therefore magnetic breakdown can occur near $\theta = 45°$ when the separation is the order of inverse magnetic length. Possible angle-dependent trajectories are demonstrated in
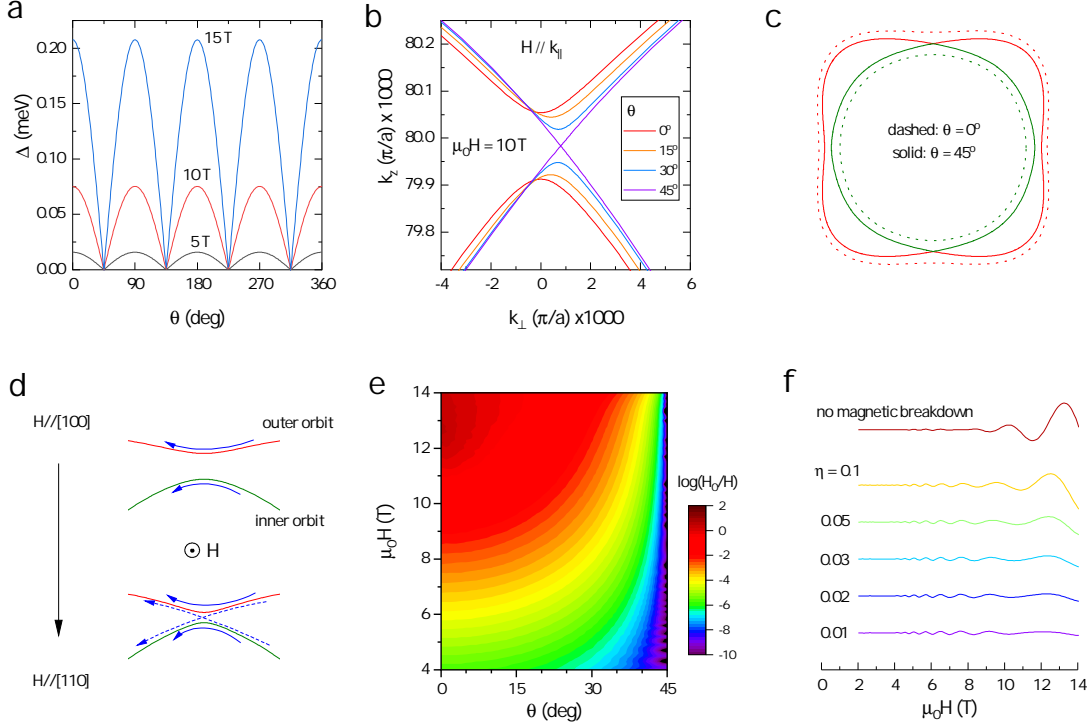
FIG. S6. Angle-dependent Zeeman interaction and quantum oscillation orbits of $j = 3/2$ Fermi surface. A magnetic field H is applied from [100] ($\theta = 0°$) to [110] ($\theta = 45°$). (a) The calculated angle-dependent Zeeman gap (Δ) exhibits strong anisotropy, and Δ vanishes at the [110]-equivalent directions; 45°, 135°, etc. (b) The corresponding Fermi surface cross sections near k_z-axis with 10 T. (c) Schematic cyclotron orbits corresponding to $\theta = 0°$ and 45°. The inner and outer Fermi surface intersect for $\theta = 45°$ due to vanishing Δ. (d) Schematic representation of possible cyclotron orbits at moderate fields. The inner and outer orbits are well separated when $H \parallel$ [100], but the probability of the inter-orbit hopping (magnetic breakdown) will increase as H approaches [110]. (e) A typical field scale for magnetic breakdown (H_0) to the actual field (H). The magnetic breakdown scenario becomes increasingly plausible near $\theta = 45°$. (f) Quantum oscillations with magnetic breakdown governed by an extra phase η across the inter-orbit gap.

Fig. S6(d). To confirm the increasing probability of magnetic breakdown, we calculate a typical breakdown field [3]

$$H_0 = \frac{\pi \hbar c}{e} \left(\frac{k_g^3}{a + b} \right)^{1/2} \tag{S1}$$

for each Fermi surface configuration. Here k_g is the closest distance between the two Fermi surfaces, and a and b are the curvature of each Fermi surfaces. Fig. S6(e) shows the numerical result for H_0/H which clearly shows that magnetic breakdown is most probable near the [110] direction.

Magnetic breakdown typically results in observation of additional QO frequencies, for example $F_1 + F_2$ or $F_1 - F_2$ in the well-studied material BEDT-TTF [4]. In our particular geometry of Fermi surface the most prominent emergent frequency from the magnetic breakdown is $(F_1 + F_2)/2$. This results from the two successive breakdown process where the cyclotron orbit consists of, for instance, green line on the left and red line on the right (or vice-versa) in Fig. S6(c). However, we do not directly observe the new frequency as the difference between the original and the emergent frequency ($\sim$5T) is smaller than the frequency resolution (6T). While measurements on higher magnetic field generally improves the frequency resolution, this is not ideal for such small Fermi surface like YPtBi as measurement up to 35T (the highest available DC field) would add less than two oscillations. Therefore, increasing the signal-to-noise level at the low field is more beneficial and can be achieved by improving the quality of a single crystal sample or employing a focused ion beam technique to fabricate the sample down to micrometer dimensions. We also note that inter-orbit hopping is prevented for a perfectly spin-orbit locked Fermi surfaces when hopping occurs at the points with same polar angle (measured in the plane perpendicular to the field) and thus consist of opposite spins. However, this is not the case for our situation since the magnetic field breaks the perfect spin-orbit locking, and the hopping occurs for a slightly different angle as seen in Fig. S6(d). As a result, the inter-orbit hopping and the possibility of

magnetic breakdown is not prevented from the spin-blockade.

When magnetic breakdown occurs, QO can be suppressed over a wide field range due to interference. To demonstrate the idea, let us assume the four main oscillatory components (inner, outer, and the two combined) have the same amplitude. (This is a bold assumption which is exact only at a certain magnetic field, and not considering less-prominent higher breakdown processes is an approximation. Therefore this is a demonstration rather than a proof.) The overall amplitude A will be proportional to

$$
\begin{aligned}
A \propto \cos[2\pi F_1/H + \phi_1] + \cos[2\pi F_2/H + \phi_2] \\
+ 2\cos[\pi(F_1 + F_2)/H + (\phi_1 + \phi_2)/2 + \eta].
\end{aligned}
\tag{S2}
$$

Here F_i and ϕ_i are frequencies and phases from the outer ($i = 1$) and inner orbits ($i = 2$), and η represent an extra phase accumulated during the inter-orbit hopping. The overall amplitude sensitively depends on η in the typical laboratory field range, and the QO can be weak for a small η for a range of parameters. Fig. S6(f) shows QO for selected η values compared to the QO without magnetic breakdown, where F_i and ϕ_i are experimentally determined at $\theta = 0°$. Since $\eta \to 0$ as $\theta \to 45°$ [5], this can explain the small QO amplitude observed in experiment. Moreover, once the magnetic breakdown is significant, there will be far more than four oscillatory components each with different phase and amplitudes, making the constructive interference even less likely.

We again emphasize that the above argument is a demonstration that the suppression of QO from magnetic breakdown is plausible, but not necessarily sufficient or definitive. The approximated equation Eq. (S2) does not identically goes to zero – Fig. S6(f) is showing that the QO amplitude given by Eq. (S2) does vanishes with the experimental parameters and field range. Also, the vanishing Δ and magnetic breakdown is not a unique feature of the $j = 3/2$ Hamiltonian, but also occurs in the $j = 1/2$ Hamiltonian as well. Therefore, the claim of $j = 3/2$ Hamiltonian and the magnetic breakdown picture should be complemented with the angle-dependence of the QO amplitude argument in the main text.

COMPARISON OF $j = 3/2$ AND $j = 1/2$ SCENARIO

Here, we present a detailed calculation of Fig. 4(c) and (d) in the main text. Note that the calculation in this section is for $H = 0$.

We consider the area of Fermi surface (FS) cross-section which is perpendicular to the field direction, $S(k_\parallel)$, where $k_\parallel$ is the momentum space distance of the plane of a cross-section from the Γ-point ($k_\parallel = 0$ for the cross-section containing the Γ point). Fig. S7(a) shows $S(k_\parallel)$ of the outer FS for $D = 0.116$ eVÅ and a number of different field directions. $\theta = 0°$ indicates the field is applied in the [100]-direction and $\theta = 45°$ is for the [110]-directional field. One can observe that when $\theta = 0$, $S(k_\parallel = 0)$ is a minimum with two maxima nearby. This is due to the bulging structure of the FS [Fig. S5] resulting from the Hamiltonian [Eq. (3) of the main text] which can also be viewed as a result of the degeneracies at the principal axes. The relative magnitude of $S(k_\parallel = 0)$ to the maximum value increases as θ grows, and $S(k_\parallel = 0)$ eventually becomes a maximum for a large enough angle. In this particular choice of parameters, this crossover occurs near $\theta = 15°$. We also calculate a similar plot for the inner FS in Fig. S7(b). Unlike the outer FS, here $S(k_\parallel = 0)$ is always a maximum regardless of θ which is consistent with the fact that the inner FS is nearly spherical.

The amplitude of the quantum oscillation depends linearly on the density of states contributing to the extremal orbits. From the Lifshitz-Kosevich formula, this is proportional to $[\partial^2_{k_\parallel} S(\tilde{k}_\parallel)]^{-1/2}$ where the tilde indicates the $k_\parallel$ value is at an extremum [3]. This formula only takes into account the second derivative of $S(k_\parallel)$ which, strictly speaking, is not sufficient for the crossover case mentioned in the previous paragraph. However, this will only contribute as a small quantitative error (say, in the value of fitted parameter D) and not affect the overall scenario. Fig. 4(c) of the main text is thus $[\partial^2_{k_\parallel} S(\tilde{k}_\parallel)]^{-1/2}$ for a single maximum and a proper summation of the contribution for the case of three extrema. The $\pi/2$ phase difference for minimum and maximum are taken into account, but we have assumed the frequencies of the minimum and maximum to be similar enough to ignore beating effects in this calculation.

Now we can calculate an analogous quantity for the $j = 1/2$ case. The most general $\mathbf{k} \cdot \mathbf{p}$ Hamiltonian (up to cubic terms of k) for the spin-half electrons respecting all symmetries are:

$$
\mathcal{H} = Ak^2 + B\sum_i k_i(k_{i+1}^2 - k_{i+2}^2)\sigma_i,
\tag{S3}
$$

where σ's are spin Pauli matrices. The parameters $A = -22.9$ eVÅ^2 and $B = 153.7$ eVÅ^2 are chosen to match the dispersion along [100] and [110] direction of the hole bands in $j = 3/2$ Hamiltonian near the chemical potential.
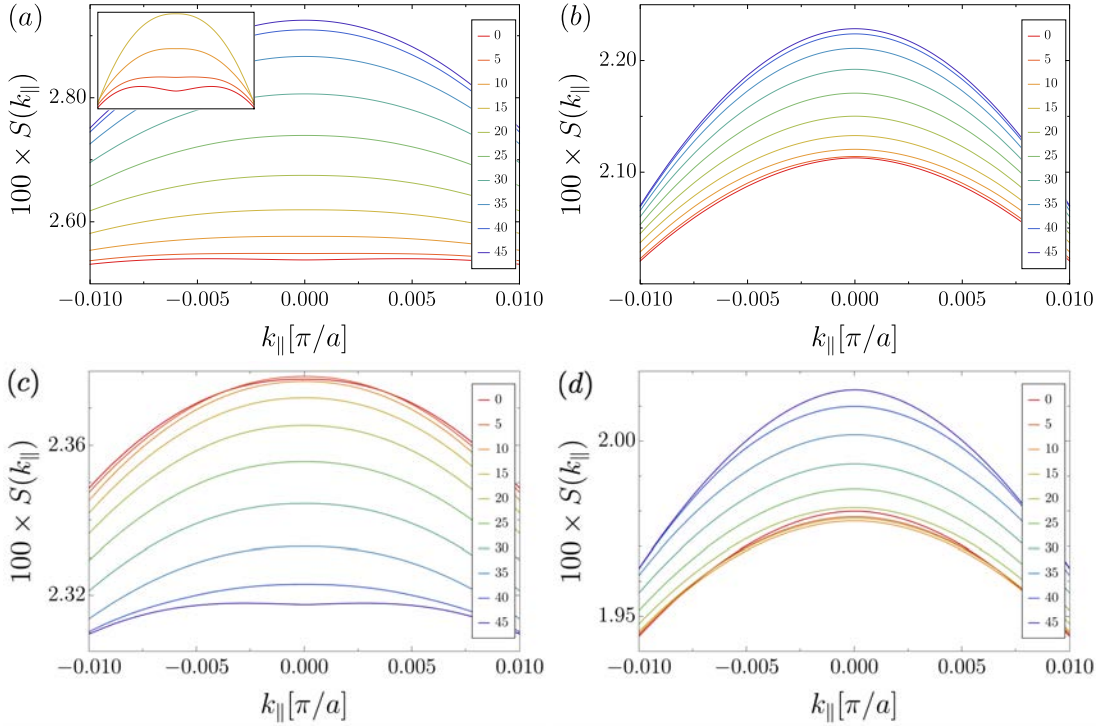
FIG. S7. $j = 3/2$ FS cross section area as a function of $k_\parallel$ for the outer [(a)] and inner [(b)] FS. The colors represents different field direction, indicated in the units of degrees. The inset of (a) is the $0°$, $5°$, $10°$, and $15°$ data vertically shifted to show that $S(k_\parallel = 0)$ is a local minimum for small angles. $j = 1/2$ FS cross section area as a function of $k_\parallel$ for the outer [(c)] and inner [(d)] FS. The inner FS shows similar trend as in $j = 3/2$, but note the crucial difference in the outer FS where the trend is reversed and local minimum at $k_\parallel = 0$ occurs at large angles.

We again calculate the $S(k_\parallel)$ for this Hamiltonian and the result is shown in Fig. S7(c) and (d). While the inner FS shows a similar trend as the $j = 3/2$, the outer FS present opposite behavior as θ increases. $S(k_\parallel)$ decreases near $k_\parallel = 0$ and becomes a minimum near $\theta = 45°$. This is due to the property of the above Hamiltonian. Unlike the $j = 3/2$ Hamiltonian which had degeneracies only at the principal axes, additional degeneracies are present along the [111] equivalent directions in the $j = 1/2$ Hamiltonian. This anti-bulging, in contrast to the bulging in $j = 3/2$, in [111]-direction results in a decrease of the FS cross-section area and is why the $j = 1/2$ in Fig. 4(d) in the main text shows peaks near $\theta = 45°$. Fig. S7(c), (d) is calculated from a particular Hamiltonian [Eq. (S3)] to keep the same order of k as in Eq. (3) in the main text, and has only two parameters to tune. However, the general trend observed in Fig. S7(c), (d) is not dependent on the order of k or the number of parameters, but is a consequence of the anti-bulging at the [111] equivalent directions of the $j = 1/2$ Hamiltonian which survives to all orders of k.

[†] These two authors contributed equally.
[*] paglione@umd.edu
[1] O. Pavlosiuk, D. Kaczorowski, and P. Wiśniewski, Superconductivity and shubnikov–de haas oscillations in the noncentrosymmetric half-heusler compound yptbi, Phys. Rev. B **94**, 035130 (2016).
[2] W. Yang, T. Xiang, and C. Wu, Majorana surface modes of nodal topological pairings in spin-$\frac{3}{2}$ semimetals, Phys. Rev. B **96**, 144514 (2017).
[3] D. Shoenberg, *Magnetic Oscillations in Metals*, Arnold and Caroline Rose Monograph Series of the American So (Cambridge University Press, 1984).
[4] J. Singleton, Studies of quasi-two-dimensional organic conductors based on BEDT-TTF using high magnetic fields, Reports on Progress in Physics **63**, 1111 (2000).
[5] A. Alexandradinata and L. Glazman, Semiclassical theory of landau levels and magnetic breakdown in topological metals, Phys. Rev. B **97**, 144422 (2018).